



# Lawrence Berkeley Laboratory

UNIVERSITY OF CALIFORNIA

## Materials & Molecular Research Division

Submitted to Acta Metallurgica

A STUDY OF PRECIPITATION IN INTERSTITIAL ALLOYS.  
I. PRECIPITATION SEQUENCE IN Ta-C ALLOYS

U. Dahmen, K. H. Westmacott and G. Thomas

August 1980

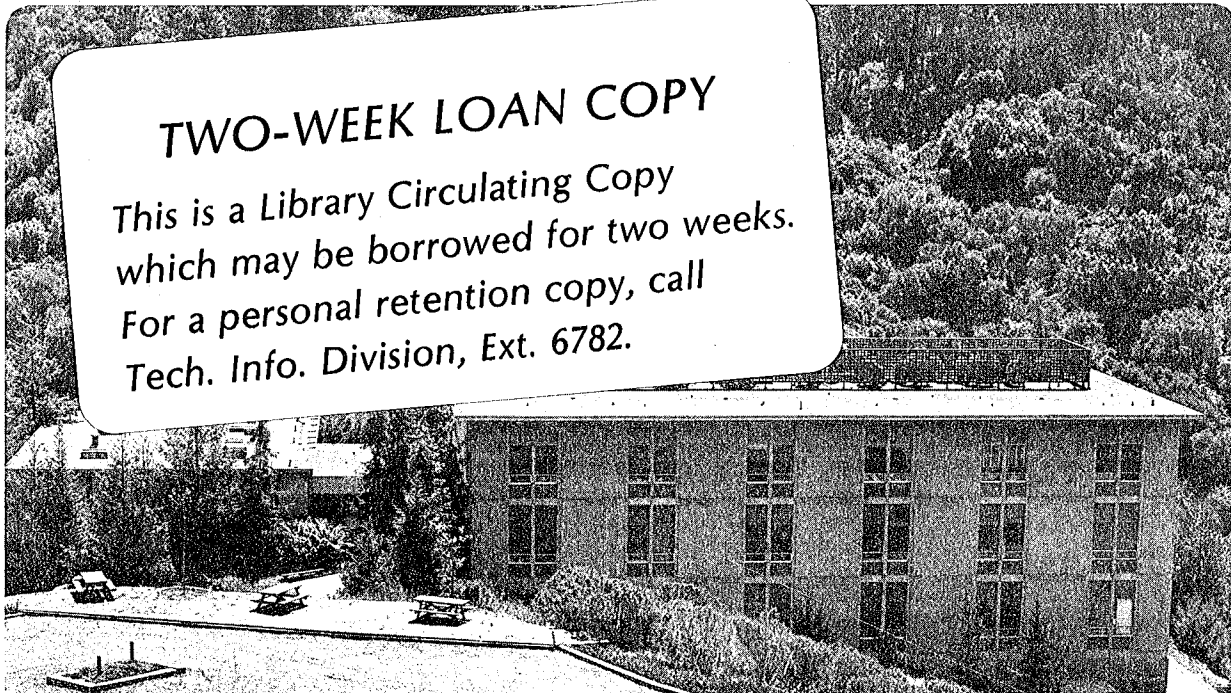
RECEIVED  
LAWRENCE  
BERKELEY LABORATORY

OCT 17 1980

LIBRARY AND  
DOCUMENTS SECTION

**TWO-WEEK LOAN COPY**

*This is a Library Circulating Copy  
which may be borrowed for two weeks.  
For a personal retention copy, call  
Tech. Info. Division, Ext. 6782.*



LBL-11244 e.2

A Study of Precipitation in Interstitial Alloys.

I. Precipitation Sequence in Ta-C Alloys

U. Dahmen, K. H. Westmacott and G. Thomas

Materials and Molecular Research Division

Lawrence Berkeley Laboratory

University of California

and

Materials Science and Mineral Engineering Department

University of California

Berkeley, California 94720



Abstract

A systematic transmission electron microscopy study of carbide precipitation in quenched-aged tantalum-carbon alloys has clarified the mechanism of precipitation in refractory BCC metal-carbon alloys. Diffraction contrast analysis shows that the precipitate platelets lie on {310} planes of the matrix, are interstitial in nature, and fully coherent before they thicken further and lose coherency. The precipitation sequence is continuous and involves no renucleation during the formation of the non-coherent phase. Thus, the final orientation relationship of the precipitate with the matrix already is found at the earliest stage at which it is possible to detect it. The interpretation of the results indicates that, as in FCC alloys, vacancies play an important role in the precipitation process during the nucleation and early growth stages and permit the formation of the hexagonal equilibrium  $M_2C$  structure early in the sequence. The model proposed to explain the observations is also consistent with the multistage hardening observed in quenched-aged refractory metal interstitial alloys.



## INTRODUCTION

In contrast to substitutional alloys comparatively few systematic studies of precipitation hardening in interstitial alloys have been undertaken. This is partly related to technological interest, but it is also because of the difficulty of introducing and maintaining controlled amounts of an interstitial element in an alloy while excluding other unwanted interstitial impurities. In the present study, transmission electron microscopy was used to follow the precipitation sequence in Ta-C alloys and the problem of purity control was circumvented by performing all the thermal treatments in a bakeable all-metal high vacuum system.

Previous work on precipitation from supersaturated FCC substitutional solid solutions has shown that the microstructure and properties are strongly dependent on the quenching and aging treatments (e.g. 1), and a similar correlation has been noted in BCC alloys. During the 1950's and 1960's TEM was used in a number of studies of quenched/aged Fe-base alloys. Substitutional Fe-Mo, Fe-Cu and Fe-Au alloys were investigated by Hornbogen<sup>(2, 3)</sup> who showed that precipitation sequences analogous to those found in FCC systems occurred. Hull and Mogford<sup>(4)</sup> observed small loop-like defects on {100} planes in quenched-aged Fe-C ferritic alloys which were interpreted as monolayer precipitates of carbon atoms analogous to GP zones, while Hale and McLean<sup>(5)</sup> and Smith<sup>(6)</sup> observed dendritic structures of carbides on dislocations in more concentrated Fe-C alloys. Smith, in fact, suggested that the carbon precipitated on dislocation loops which formed from the quenched-in vacancies. The effect of substitutional additions to binary Fe-C alloys was studied by Leslie<sup>(7)</sup>, and changes in the carbide precipitation temperature were explained in terms of variations in C activity with alloying.

Comprehensive studies of ternary alloys based on Fe-N have been published in a series of classical papers by Jack and co-workers<sup>(8)</sup>. In 1972 a significant advance in understanding  $\epsilon$ -carbide precipitation in ferrite was made by Vyhnal and Radcliffe<sup>(9)</sup> (VR). They found a striking increase in the number of carbide particles precipitated at high quenching rates compared to low rates and developed a semi-quantitative model in which post-quench carbide nucleation occurred on single vacancy-carbon atom complexes formed at the solution treatment temperature. More recently some systematic studies of quench-aged refractory metal carbon alloys have been made by Diercks and Wert<sup>(10)</sup> and Viswanadham and Wert<sup>(11)</sup> finding carbide precipitation to be a multistage process similar to an aging sequence in substitutional Al-alloys. It is a well-known fact that quenched-in vacancies enhance diffusion and promote zone formation in FCC substitutional alloys, but their possible role in BCC alloy systems was obscured by the difficulty in obtaining unambiguous evidence for significant retained vacancy concentrations in quenched BCC metals.<sup>(12)</sup> The present results have further clarified this aspect and when considered together with concurrent developments in the understanding of carbon-vacancy interactions in FCC metals<sup>(13)</sup>, a recent new theoretical treatment of vacancy retention in impure quenched metals<sup>(14)</sup>, and the earlier work of VR provide the framework for a model which may be applicable to a wide variety of systems. Both the observed microstructures and the known mechanical properties of quenched-aged Ta-C and other refractory metal precipitation hardening alloys are in excellent accord with this model.

In this paper, the sequence of events which leads to the formation of the stable Ta<sub>2</sub>C phase is described. A detailed description of

the transition from coherent to incoherent precipitates and the orientation relationship, and a theoretical continuum/discrete lattice analysis of the entire phase transformation are treated in separate papers.

### Sample Preparation

The material was prepared from 99.9 wt.% pure tantalum by electron beam zone-refining. After three passes the single crystal rod of 8mm diameter was rolled into a sheet of 150 $\mu$ m thickness. Small strips were cut from this sheet and carburized to a concentration of about 0.5 at.% at 2000 $^{\circ}$ C first by coating with graphite and later by reaction with acetylene gas. (For a more detailed account of the sample preparation, see refs. 15, 16). Samples 25 x 3 x 0.15mm were outgassed and homogenized in ultrahigh vacuum  $\sim 10^{-6}$  Pa by Joule heating with ac current prior to quenching. The samples were subsequently aged without breaking the vacuum. Discs of 3mm diameter were cut from the center of each sample and thinned for electron microscopy in a double jet polisher using an electrolyte of 4 vol.% H<sub>2</sub>SO<sub>4</sub> in methanol at  $-30 \pm 5^{\circ}$ C and a current density of 1Acm<sup>-2</sup>. The electron microscopy was done on various 100kV microscopes.

### Results

The quenching rate of  $\sim 2500^{\circ}$ Cs<sup>-1</sup> achieved in the ultrahigh vacuum quenching apparatus<sup>(17)</sup> was sufficient to produce a supersaturated solution of carbon in tantalum. Fig. 1 shows an example of such a quenched foil. Note the strong mottling of the background, an effect which was not observed in the fully aged foils polished under identical conditions. Only a few isolated dislocations were present.

(i) Precipitate Morphology

Aging a quenched foil in UHV at  $\sim 450^{\circ}\text{C}$  for 144h produced a high density of small, platelike precipitates, as shown in fig. 2. Trace analysis showed their habit planes to be the  $\{310\}$  planes of the matrix. This can be seen in fig. 2 where the beam direction was near  $[001]$ . The traces of the four  $\{310\}$  planes contained in the  $[001]$  zone are indicated in the figure and the corresponding four sets of precipitates which are seen edge-on are easily recognized. Because there are twelve crystallographically equivalent  $\{310\}$  planes in a cubic crystal, the precipitate habit appeared almost random. Similar platelike precipitates on  $\{310\}$  habit planes have been found in the Nb-C and V-C systems under equivalent aging conditions<sup>(10, 11)</sup> as well as in the ternary systems Mo-Ti-C and Mo-Ti-N.<sup>(18)</sup>

The volume density of precipitates was on the order of  $10^{15}\text{cm}^{-3}$  and their distribution was homogeneous except near lattice defects such as dislocations, grain and interphase boundaries. Examples of precipitate-free zones (PFZ's) near lattice imperfections are shown in fig. 3. Very small PFZ's were observed near dislocations as in fig. 3a. Apparently the dislocation, which is out of contrast in this micrograph, has served as a preferred nucleation site for precipitate plates in two of the twelve  $\{310\}$  orientations. The large straight undissolved carbide precipitate visible in fig. 3b exhibits a much more pronounced PFZ. Such zones were found at all matrix/ $\text{Ta}_2\text{C}$ -carbide interphase boundaries and had a uniform width of about  $0.1\mu\text{m}$ . The widest PFZ's were observed along grain boundaries. Fig. 3c shows a  $1\mu\text{m}$  wide zone on either side of the grain boundary traversing the micrograph. The phenomenon of PFZ's near lattice defects has frequently been observed

in quench-aged Al alloys and is generally attributed to vacancy depletion. The different precipitate sizes and densities in figs. 2 and 3 were the result of a variation in aging time and temperature as described later.

(ii) Contrast Analysis

In order to understand the nucleation and growth of these coherent precipitates, detailed diffraction contrast and spot pattern analyses were performed. It was noticed that in certain orientations and diffracting conditions the precipitate platelets of fig. 2 showed contrast similar to dislocation loops (as is well-known and expected for thin plates). This is illustrated in fig. 4 which shows the same foil as fig. 2 after a large tilt of the specimen to a  $[101]$  beam direction. The effect of the precipitates on the surrounding matrix could be determined by using the loop analogy, i.e. the sign, size and direction of the matrix strain produced by the precipitate was analysed by conventional methods of dislocation loop analysis in TEM. Such a contrast analysis is shown in fig. 5. "Loops" on different types of  $\{310\}$  planes are marked A, B, and C. Figures 5a-d are images taken with different  $\underline{g}$  vectors around the  $[001]$  pole. Figures 5e and f are a plus/minus  $\underline{g}$  pair taken near the  $[101]$  pole. By trace analysis, and from the change in the projected image width upon tilting, it was determined that "loop" A had  $(310)$  habit, "loop" B was on  $(301)$  and C on  $(103)$ . If the strength of contrast is taken as a measure of the product  $\underline{g} \cdot \underline{R}$ , where  $\underline{R}$  is the displacement vector of the loop, then a semi-quantitative value for the magnitude and direction of  $\underline{R}$  can be obtained from the systematic contrast variation with  $\underline{g}$ -vector. By comparison with images of real prismatic dislocation loops in the same

material, the contrast of "loops" A, B and C in figs. 5e and f roughly corresponds to  $g \cdot R_{\sim} = 1$  with A slightly stronger than B and C. As seen by comparison with table 1 the contrast variation in fig. 5a-f is consistent with a displacement vector  $R_{\sim}$  nearly perpendicular to the habit plane with magnitude of roughly  $1/3 \langle 310 \rangle$ .

Table 1

Predicted contrast behavior of precipitates assuming displacement vectors of type  $1/3 \langle 310 \rangle$  showing good agreement with the contrast experimentally observed in fig. 5.

Loop	$R_{\sim}$	$g \bar{1}\bar{1}0$	$g \bar{2}00$	$g 1\bar{1}0$	$g 0\bar{2}0$	$g 10\bar{1}$
A	$\pm \frac{1}{3} [310]$	$\pm \frac{4}{3}$	$\pm 2$	$\pm \frac{2}{3}$	$\pm \frac{2}{3}$	$\pm 1$
B	$\pm \frac{1}{3} [301]$	$\pm 1$	$\pm 2$	$\pm 1$	0	$\pm \frac{2}{3}$
C	$\pm \frac{1}{3} [103]$	$\pm \frac{1}{3}$	$\pm \frac{2}{3}$	$\pm \frac{1}{3}$	0	$\pm \frac{2}{3}$

The sign of the displacement vector  $R_{\sim}$  can be determined unambiguously from the inside/outside contrast effect as described by Groves and Kelly<sup>(19)</sup> and more recently by Föll and Wilkens,<sup>(20)</sup> see appendix.

According to this analysis all the "loops" were interstitial in nature, as expected for precipitates of increased atomic volume.

In summary, the contrast behavior of the precipitates in the loop analogy was that of a faulted interstitial near-edge dislocation loop

with a Burgers vector of approximately  $a/3 \langle 310 \rangle$ . Assuming that this displacement was caused by the expansion due to formation of a coherent precipitate with a volume increase of about 15% (as in the equilibrium carbide  $Ta_2C$ ), and assuming this volume increase to be accommodated entirely in the direction normal to the loop plane, a lower limit of  $\sim 2$  nm could be placed on the thickness of the precipitates at this stage. An upper limit was obtained from an estimate of the length of the reciprocal lattice rods normal to the habit plane, this length being inversely proportional to the precipitate thickness. A dark field image as in fig. 6 which was taken with a (110) reflection tilted about  $16^\circ$  (or  $1 \text{ nm}^{-1}$ ) away from the Ewald sphere shows that the intensity in this configuration arose almost exclusively from precipitates seen face-on. According to the kinematical expression for the shape factor<sup>(21)</sup>, this means that the maximum thickness of the platelets in this stage was  $\sim 2 \times (1 \text{ nm}^{-1})^{-1}$ , or 2 nm, the same as the lower limit estimated above. Hence it was concluded that a quench-aging treatment at  $\sim 450^\circ\text{C}$  for 144h produced a high density of platelike precipitates on {310} habit planes, about 30 nm in diameter and  $\sim 2$  nm thick.

### (iii) Effect of Aging Treatment

Under different aging conditions both the diameter and the thickness of the precipitates changed. Figure 7 shows the carbides obtained by aging for 75h at  $\sim 450^\circ\text{C}$ . Their size was about 10 nm and even though the habit plane was the same as for the large carbides, the contrast under similar diffracting conditions was weaker (cf. figs. 4 and 7). Upon aging at the higher temperature of about  $550^\circ\text{C}$ , the precipitates grew to a size of about 50 nm as shown in fig. 8. The large strain lobes around the precipitates are evidence for the substantial elastic strains necessary to maintain coherency with the

matrix. In addition to their lateral growth, the platelets had thickened and lost their dislocation loop-like character. They were also no longer in good alignment with the  $\{310\}$  planes. Their size was now large enough to obtain diffraction patterns by convergent beam microdiffraction. This is shown in fig. 9 where the extra spots due to the coherent precipitate are outlined. By comparison with the analysis of the later stages of precipitation<sup>(22)</sup>, these patterns were found to arise from the hexagonal structure of the equilibrium carbide  $Ta_2C$ . The orientation relationship for the coherent carbide was the same as that for the non-coherent carbide. Superlattice spots due to ordering of the carbon in alternate (0001) layers are marked by arrows in fig. 9.

The experimental evidence presented can be summarized as follows:

-during aging of rapidly quenched Ta-C alloys, coherent carbides were precipitated in the matrix with high density and homogeneous distribution.

-the precipitates were platelike in shape and had a  $\{310\}$  habit.

-before losing coherency, the carbides could grow to at least 50 nm in size.

-the structure and orientation relationship of the coherent carbide was that of the equilibrium carbide  $Ta_2C$ .

-the large coherent carbides were faulted and often deviated from the  $\{310\}$  habit.

-the smaller precipitates could be described either by analogy with dislocation loops, as faulted interstitial loops with a Burgers vector of about  $1/3 \langle 310 \rangle$ , or as hexagonal precipitates of  $\sim 30$  nm diameter and  $\sim 2$  nm in thickness.

-precipitate-free zones near dislocations, interphase boundaries and grain boundaries were found for all aging treatments.

## DISCUSSION

It is advantageous to discuss the precipitation sequence in an order reverse to that in which it develops chronologically. By tracing back from the large coherent carbides to the nucleation event, an understanding of the entire precipitation sequence is made possible.

As shown by the convergent beam microdiffraction experiments, the crystal structure of the large coherent carbides is identical to the ordered hexagonal structure of the equilibrium carbide  $Ta_2C$ . It is therefore not necessary for the precipitates to re-nucleate during the loss of coherency. This is consistent with the experimental observations here as well as the studies of Diercks and Wert<sup>(10)</sup> (DW) on V-C and Viswanadham and Wert<sup>(11)</sup> (VW) on Nb-C, who also found that the incoherent precipitates formed directly from the coherent carbide. In contrast to the present result, however, these authors concluded that the transition was accompanied by a change in crystal structure of the precipitate. This is clearly not the case in the Ta-C system. Indeed, there is no experimental evidence for a structural transformation at any stage of the precipitate growth; nor is there any reason to believe that such a transformation is necessary. Hence, it is concluded that the precipitate structure is already hexagonal following nucleation.

The consequences of this conclusion will now be examined in the light of the experimental evidence available for the Ta-C and other alloy systems.

The coherent carbide observed in the present study appears to be identical to the ones reported by DW for V-C<sup>(10)</sup> and VW for Nb-C<sup>(11)</sup> alloys subjected to comparable quench-aging treatments. These authors found the same characteristic features including plate shape,  $\{310\}$  habit plane and homogeneous distribution. They concluded that the

coherent carbide had an approximately BCC lattice with possibly a slight tetragonality due to carbon ordering. If this was the case, the observed  $\{310\}$  habit plane should be dictated by the elastic anisotropy. However, while Nb and V both have anisotropy ratios smaller than unity ( $A_{Nb} = 0.55$ ,  $A_V = 0.78$ )<sup>(23)</sup>, Ta has an elastic anisotropy of  $A_{Ta} = 1.56$ . In spite of this large difference, the three systems exhibit the same  $\{310\}$  carbide morphology. Clearly, the anisotropy of the matrix elastic constants cannot be of major importance. On the other hand, crystallographically the three systems are very similar, e.g.,

- i) In each case the coherent precipitates finally give way to the non-coherent equilibrium carbide of composition  $M_2C$  with a hexagonal metal sublattice.<sup>(24)</sup>
- ii) The formation of these carbides is accompanied by a comparable volume expansion of 16.5% (V), 17.1% (Nb) and 14.6% (Ta).
- iii) The transition from the coherent to the non-coherent carbide does not involve re-nucleation.
- iv) In all three alloys the equilibrium carbide follows the same orientation relationship with the matrix.

All of these facts suggest that the initial precipitation on the  $\{310\}$  habit plane is a consequence of an underlying crystallographic relationship. This does not contradict the well-established theories for coherent elastic inclusions which state that two of the variables determining the elastic strain energy of a precipitate are the strain and the elastic anisotropy.<sup>(25)</sup> The usual treatment assumes a simplified strain, e.g. a tetragonal distortion or a uniaxial expansion, and a realistic elastic anisotropy, whereas the experimental evidence presented here suggests that it is valid to assume simple elastic

isotropy and necessary to use a more complex, realistic description of the strain.

A direct experimental verification of this is shown in fig. 10. The high resolution lattice fringe image of a coherent carbide precipitate taken near the thin edge of a tantalum foil shows directly the shear of the close-packed  $\{110\}$  planes as they cross the precipitate. The measured amount of shear is  $10^0$ , too large to be neglected if a simple tetragonal distortion is assumed. This latter description is used by DW when analysing the lattice of the coherent carbide in vanadium as tetragonally distorted BCC. However, a tetragonal distortion cannot explain the observed shear, and if the precipitate is described as elastically strained BCC, a more general strain must be used. In view of the evidence discussed above, the present study describes the coherent carbide lattice as a distorted hexagonal structure. Of course, both points of view--that of a strained BCC lattice and that of a strained HCP lattice--must be equivalent since each lattice plane and every atom in the matrix structure must be matched in the precipitate, as implied in the concept of coherency.<sup>(26)</sup> The description used here, however, says that the relaxed precipitate structure would be HCP and shows that only a mixed strain involving both shear and expansion can accurately reflect the real coherency distortion. This point will be examined in detail in a separate publication.

With this new and more accurate description of the coherent carbide in mind, it is interesting to evaluate some of the other experimental observations obtained here and in previous studies. As shown in fig. 3, precipitate-free zones (PFZ's) were found near dislocations, interphase and grain boundaries. Such PFZ's have often been reported to occur in quench-aged Al-alloys<sup>(1)</sup> as well as Fe-base

alloys<sup>(27)</sup> and are ascribed to the presence of vacancy gradients near sinks. In the case of Ta-C alloys, due to the high mobility of both vacancies and interstitial carbon,<sup>(12)</sup> it is possible that a depletion of either the carbon solute or the lattice vacancies is responsible for the PFZ's. However, the fact that no heterogeneous nucleation was observed at the grain boundaries which exhibited PFZ's points to vacancy depletion as the mechanism which prevents nucleation in a PFZ. Therefore, it may be concluded that lattice vacancies are essential to the formation of a carbide nucleus. The role of vacancies in precipitation phenomena has been discussed from a thermodynamics point of view by Russell<sup>(28)</sup> and Khachatryan.<sup>(29)</sup> Russell has shown that excess vacancies can drastically influence the nucleation rate of misfitting precipitates. The large (14.6%) volume increase associated with the formation of the carbides in tantalum is likely to provide a strong attraction for vacancies. Furthermore, it is now well-established that a strong binding exists between interstitial solute atoms and lattice vacancies due to their opposite strain fields. Experimental<sup>(30)</sup> and theoretical<sup>(31)</sup> studies agree on large binding energies on the order of 0.5 eV. As has been pointed out for example by Wert<sup>(32)</sup>, a strong binding between vacancies and impurities can greatly increase the number of vacancies retained during a quench. Thus, it appears that due to the binding to carbon atoms, vacancies can be retained in a concentration sufficient to make "heterogeneous" nucleation, i.e., the formation of a carbide nucleus with the aid of vacancies, the dominant mode of precipitation. While this is in full agreement with the experimental observations, it does not clarify the structural role of the vacancies.

It is so far unclear whether the vacancies retain their identity within the precipitate or whether they "precipitate" themselves,

leading to a local collapse of the lattice and thus a possible structural change. In the former case the particle remains coherent in the sense of Olsen and Cohen's definition<sup>(26)</sup>, whereas the case of a local lattice collapse results in a semicoherent precipitate. In this line Westmacott and Pérez<sup>(13)</sup> have explained the formation of semicoherent precipitates in Pt-C alloys by the co-precipitation of carbon and vacancies, and a similar mechanism is implied in the interaction of solute atoms with vacancy dislocation loops, as described by Hornbogen<sup>(3)</sup> for Fe-Mo and by Mitchell<sup>(33)</sup> for Mo-Hf-N alloys. Considering such a partial collapse of the lattice for the present case of Ta-C alloys, it is clear that at some early stage of precipitation the carbide should be semi-coherent and have a vacancy type strain field. An attempt to verify this directly on the smallest precipitates observed (fig. 7) failed because their small size made a unique identification of a given precipitate in a large angle tilt experiment difficult. Because of the small spacing of the {310} lattice planes, a verification by direct lattice fringe imaging was also impossible. Yet it is conceivable that at this or an earlier stage of the precipitation, the particles are semi-coherent.<sup>(25)</sup>

The local collapse of vacancies on {310} matrix planes accompanied by the simultaneous precipitation of carbon could constitute a nucleus with the carbide structure and a net strain field of vacancy type. As a consequence of such a mechanism, the precipitation would undergo several stages due to the reversal of the net strain field during precipitate growth. In a systematic study of age-hardening in rapidly quenched V-C and Nb-C, Chang et al.<sup>(34)</sup> indeed found four distinct stages of age-hardening before the carbides lost coherency. They were unable to detect any differences in the precipitate morphology and

structure which could be correlated to the various age-hardening peaks. On the basis of electrical resistivity measurements, they concluded that almost no carbon was left in solid solution by the time the first hardness peak was reached. The activation energy of the aging process was that for carbon diffusion and they found no energy barrier to nucleation. All of these findings are in good agreement with the suggested role of vacancies during the nucleation of carbides.

If, on the other hand, the vacancies retain their identity throughout the process of precipitation, they have no structural role as described above. Their significance in this case lies mainly in the partial accommodation of coherency stresses. The precipitates would be fully coherent during the entire sequence, and no explanation could be given for the reported age-hardening behavior. Both modes of vacancy assisted nucleation are consistent with all the other experimental observations and it seems clear that vacancies play a critical role in the formation of the carbide precipitates.

Finally, it is interesting and instructive to compare the present results on Ta with those obtained by VR on Fe. In the case of Fe, a single carbon atom-vacancy complex apparently provided an effective nucleation site at 25<sup>0</sup>C, though not at 100<sup>0</sup>C. Crystallographic analysis of the precipitate habit plane was not performed, but it was noted that the habit plane (at 25<sup>0</sup>C) appeared to be random. This is in contrast to the characteristic  $\{100\}_{\alpha}$  habit normally associated with  $\epsilon$ -carbide, and suggests perhaps that the room temperature precipitates are a precursor to  $\epsilon$ -carbide formation and lie on  $\{103\}$  planes also. Thus the emerging picture is one in which retained vacancies play a pivotal role in the nucleation and early growth stages of precipitation in a wider range of alloy systems than hitherto suspected.

At one extreme, a single vacancy-carbon atom pair is sufficient to initiate precipitation (e.g. Fe-C), while at the other, the process of graphitization (i.e. precipitation of a pure interstitial substance) would appear to require a one to one precipitation of vacancies and solute atoms. Ta(C) and other refractory metal interstitial alloys apparently represent intermediate cases where a number of vacancies reduce the nucleation barrier sufficiently to allow precipitation of the stable hexagonal structure from the outset. A more detailed discussion of these aspects will be given in a later paper.

#### SUMMARY AND CONCLUSIONS

On the basis of new experimental evidence, a mechanism is suggested for the "homogeneous" precipitation of carbides in quench-aged refractory metals. The crystal structure of the coherent carbide is the hexagonal lattice of the non-coherent equilibrium ( $Ta_2C$ ) phase. The observed  $\{310\}$  habit of the coherent carbide platelets is discussed in terms of the elastic anisotropy of the matrix and the structure of the precipitate. It is concluded that vacancies play an important part in the nucleation due a strong carbon vacancy binding as well as the large volume increase which accompanies the formation of a precipitate. The suggested mechanism is consistent with the experimental evidence presented here and in other publications on refractory metals.

#### ACKNOWLEDGEMENT

This work was supported by the Division of Materials Sciences, Office of Basic Energy Sciences, U. S. Department of Energy under Contract Number W-7405-Eng-48.

REFERENCES

1. A. Kelly and R. B. Nicholson, Progr. in Mat. Science 10, 149 (1963).
2. E. Hornbogen, Acta Met. 10, 525 (1962).
3. E. Hornbogen, J. Appl. Phys. 32, 135 (1961).
4. D. Hull and I. L. Mogford, Phil. Mag. 6, 535 (1961).
5. K. F. Hale and D. McLean, Nottingham Conference of the Institute of Physics Electron Microscopy.
6. E. Smith, Annual EMSA Meeting (1960).
7. W. C. Leslie, Acta Met. 9, 1004 (1961).
8. K. H. Jack, "Heat Treatment '73", Proc. Conf. Joint Committee Iron and Steel Inst., Inst. Metals, Inst. Metall. London, Dec. (1973).
9. R. F. Vyhnal and S. V. Radcliffe, Acta Met. 20, 435 (1972).
10. D. R. Diercks and C. A. Wert, Met. Trans. 3, 1699 (1972).
11. R. K. Viswanadham and C. A. Wert, J. Less-Comm. Metals 48, 135 (1976).
12. J. Nihoul, "Vacancies and Interstitials in Metals", eds. A. Seeger et al., Wiley Interscience (1970).
13. K. H. Westmacott and M. I. Pérez, J. Nucl. Mat. 83, 231 (1979).
14. J. A. Wert, Acta Met. to be published
15. U. Dahmen and G. Thomas, Scr. Met. 13, 527 (1979).
16. U. Dahmen, Ph. D. Thesis, U. C. Berkeley, 1979.
17. K. H. Westmacott and R. L. Peck, J. Phys. E. Scientific Instr. 9, 521 (1976).
18. N. E. Ryan, W. A. Soffa, and R. Crawford, Metallography 1, 195 (1968).
19. G. W. Groves and A. Kelly, Phil. Mag. 6, 1527 (1962).

20. H. Föll and M. Wilkens, *Phys. Stat. Sol. (a)* 31, 519 (1975).
21. P. B. Hirsch, A. Howie, R. B. Nicholson, D. W. Pashley and M. J. Whelan, "Electron Microscopy of Thin Crystals", Butterworth, London (1965).
22. U. Dahmen and K. H. Westmacott, Proc. 17th University Conf. on Ceramics, "Surfaces and Interfaces in Ceramic and Ceramic-Metal Systems, Berkeley, 1980, to be published.
23. Hirth Lothe, "Theory of Dislocations", McGraw Hill (1968).
24. E. K. Storms, "The Refractory Carbides", Academic Press, N. Y. (1967).
25. J. W. Christian, "The Theory of Transformations in Metals and Alloys", Pergamon Press, N. Y. (1965).
26. G. B. Olson and M. Cohen, *Acta Met.* 27, 1907 (1979).
27. A. S. Keh and W. C. Leslie, *Materials Science Research* 1, 208 (1968).
28. K. C. Russell, *Scr. Met.* 3, 313 (1969).
29. A. G. Khachaturyan, *Sov. Phys.-Solid State* 13, 2024 (1972).
30. M. Mondino and A. Seeger, *Scr. Met.* 11, 817 (1977).
31. M. S. Blanter and A. G. Khachaturyan, *Met. Trans.* 9A, 753 (1978).
32. J. A. Wert, *Acta Met.* to be published.
33. J. B. Mitchell, *Acta Met.* 19, 1063 (1971).
34. H. Y. Chang, R. K. Viswanadham, and C. A. Wert, *Met. Trans.* 5, 1907 (1974).
35. B. Edmondson and G. K. Williamson, *Phil. Mag.* 9, 277 (1964).

## Appendix

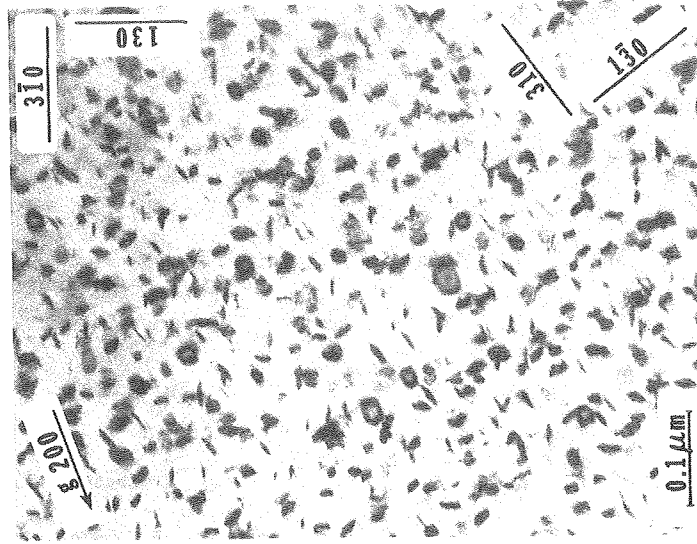
One of the main sources of error in the contrast analysis of dislocation loops has been the  $180^\circ$  ambiguity of the diffraction patterns. The method described here avoids this problem by making use of the large angle tilt capability of most modern microscopes. The foil is tilted until the loops under observation are viewed edge-on as seen in fig. 11 in an (001) pole with  $g \ 0\bar{2}0$ . By tilting the foil from this pole through a large angle, the loops show inside/outside ring contrast, as in fig. 11 after a  $45^\circ$  tilt to the (011) pole. If the direction of positive  $g$  is then defined as pointing towards the original pole in the diffraction pattern (see drawing in fig. 11), then the following simple rule holds for the contrast of edge or near-edge loops in bright field pictures with positive excitation errors.

If the loops show outside contrast when imaged with positive  $g$ , they are interstitial. Vacancy loops show outside contrast in negative  $g$ . Obviously the carbide precipitates marked A and B in fig. 11 show the contrast behavior of interstitial dislocation loops. The rule given above is similar in principle to the method proposed much earlier by Edmondson and Williamson<sup>(35)</sup> and follows directly from the analysis and definitions of Föll and Wilkens<sup>(20)</sup> with the practical advantage of being independent of the relative rotations between image and diffraction patterns.

Figure Captions

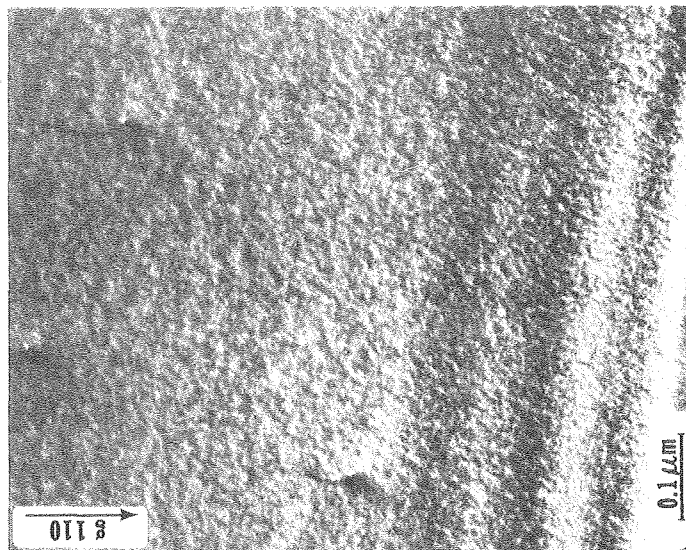
- Fig. 1 Ta  $\sim$  0.5 at.-% C alloy in as quenched condition. Note the mottled background and precipitate-free dislocations.
- Fig. 2 Coherent platelike precipitates on {310} planes of the matrix with  $[001]$  beam direction. The traces of the four {310} planes seen edge-on are marked. Ta  $\sim$  0.5at.-%C, quenched and aged 144h at  $\sim$  450 $^{\circ}$ C.
- Fig. 3 Precipitate-free zones in quench-aged Ta  $\sim$  0.5 at.-% C alloy
- a) near a dislocation (aged 75h at  $\sim$  450 $^{\circ}$ C)
  - b) near a large undissolved equilibrium precipitate visible as a dark band (heat treatment as in a))
  - c) near a grain boundary (aged 17h at  $\sim$  550 $^{\circ}$ C)
- Fig. 4 Precipitates as in fig. 2, seen near a  $[101]$  beam direction. Note the loop-like appearance.
- Fig. 5 Contrast analysis of the precipitates shown in figs. 2 and 4. The beam direction is  $[001]$  in a, b, c, d and  $[101]$  in e and f. Compare contrast variation to table 1 and note inside/outside contrast in e and f. All micrographs are bright field images with s positive.
- Fig. 6 Dark field picture using the streaking parallel to the beam direction. Only precipitates nearly perpendicular to the beam appear bright. Material as in figs. 2, 4, 5.
- Fig. 7 Small coherent precipitates after aging 75h at  $\sim$  450 $^{\circ}$ C. The beam direction is  $[111]$ .
- Fig. 8 Coherent precipitates after 17h at  $\sim$  550 $^{\circ}$ C. The strain lobes indicate large coherency strains.

- Fig. 9 Convergent beam microdiffraction patterns of precipitates as shown in fig. 8. The orientations of the matrix are (110) and (001). Extra spots arising from the precipitates are outlined in white and arise from the hexagonal  $Ta_2C$  structure. Spots due to carbon ordering are marked by arrows.
- Fig. 10 Lattice fringe image of coherent carbide precipitate at the edge of a thin foil. A shear of  $10^0$  is clearly visible from the change in fringe direction between matrix M and precipitate P. Material as in fig. 2.
- Fig. 11 Simplified contrast analysis to determine the nature of a dislocation loop (here precipitates as in fig. 2). The precipitates A and B seen edge-on in an  $[001]$  pole show outside contrast in positive  $g$  ( $g$   $01\bar{1}$ ) and are therefore interstitial in character.



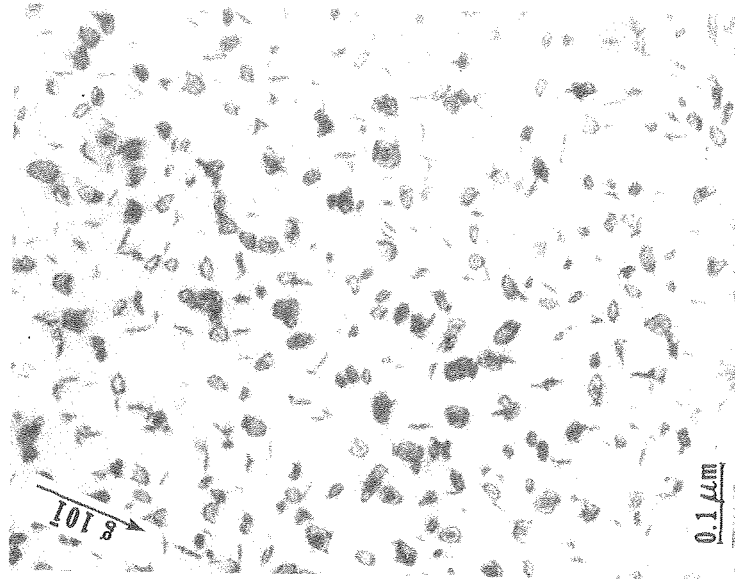
XBB 807-8730

Fig. 2



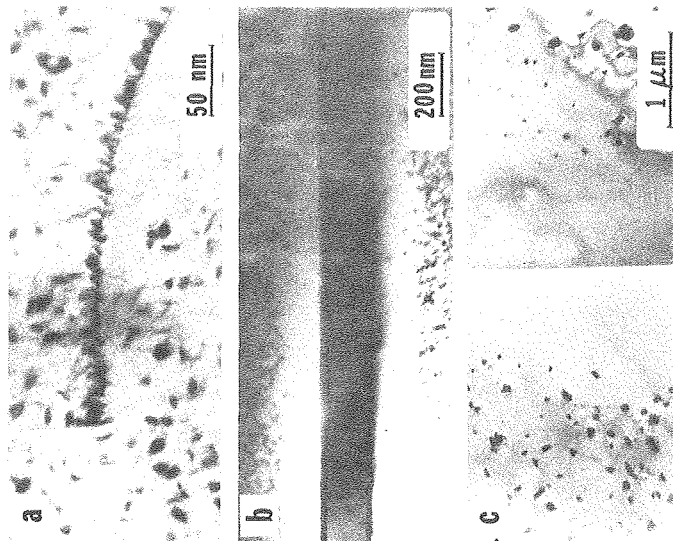
XBB 807-8729

Fig. 1



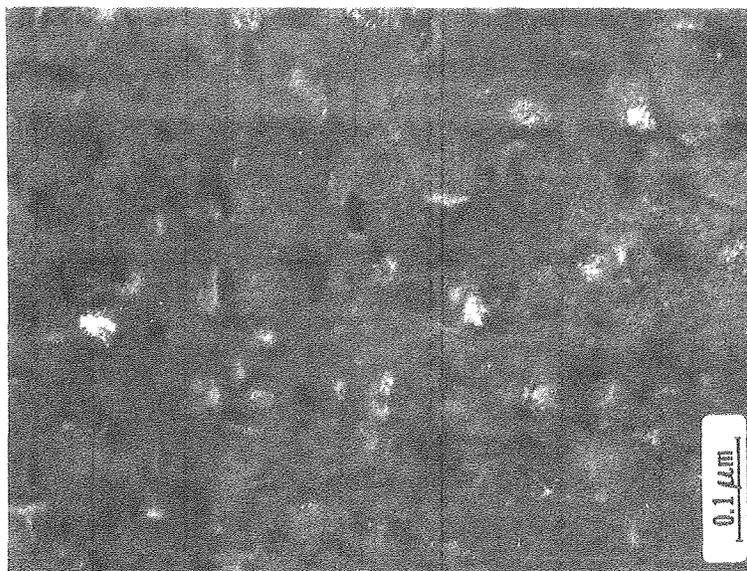
XBB 807-8732

Fig. 4



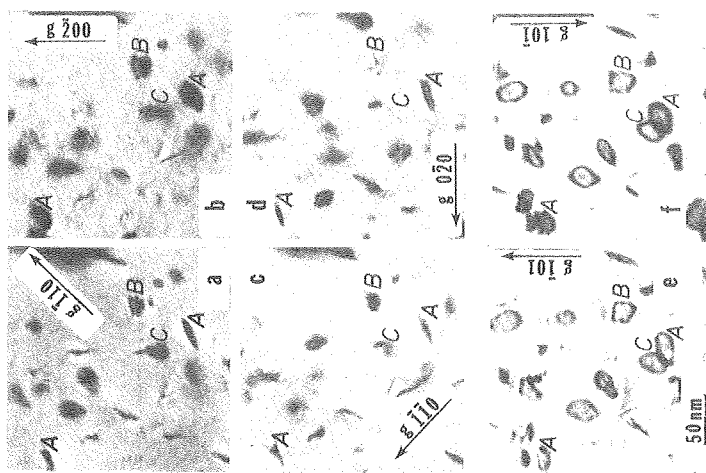
XBB 807-8731

Fig. 3



XBB 807-8733

Fig. 6



XBB 807-8738

Fig. 5

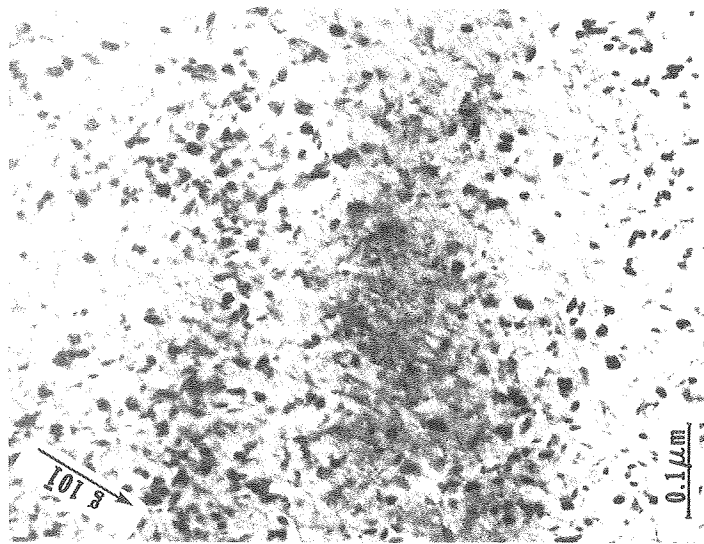


Fig. 7 XBB 807-8734

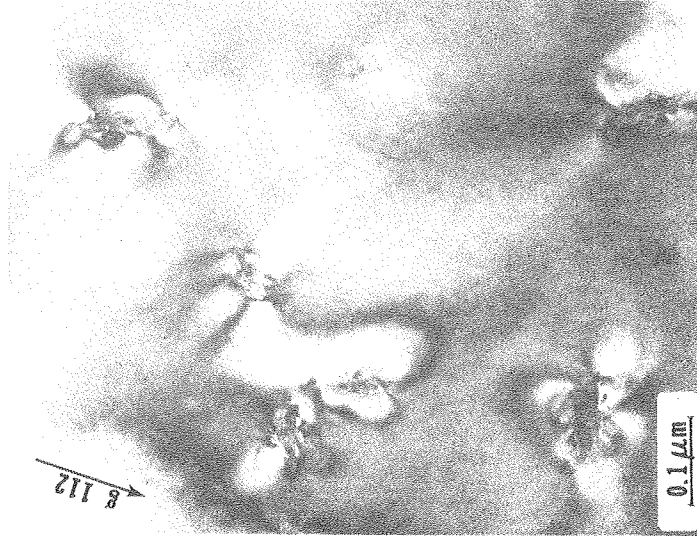
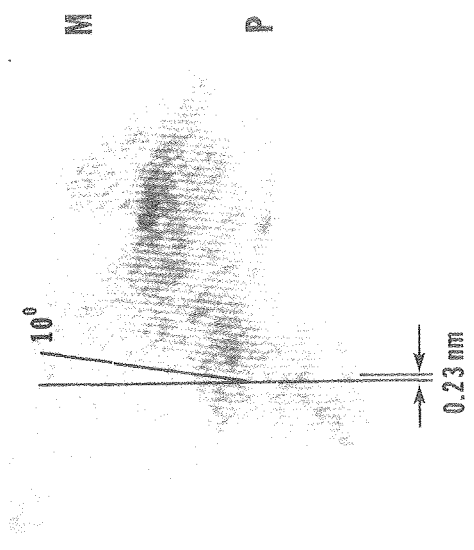
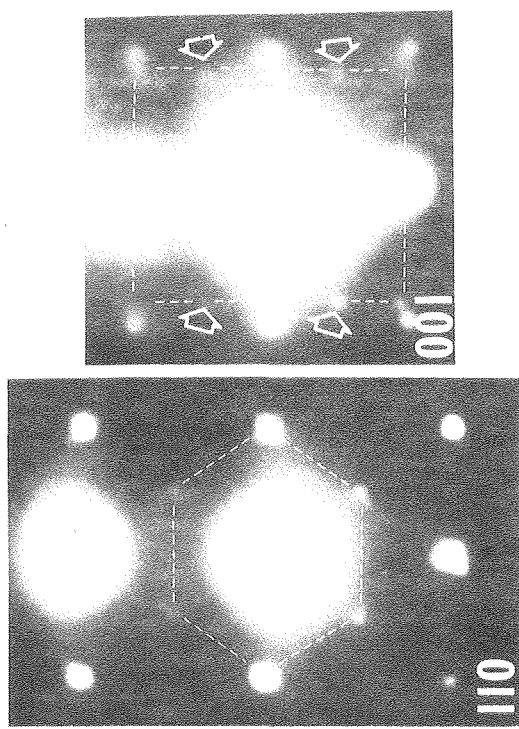


Fig. 8 XBB 807-8735



XBB 807-8737

Fig. 10



XBB 807-8736

Fig. 9

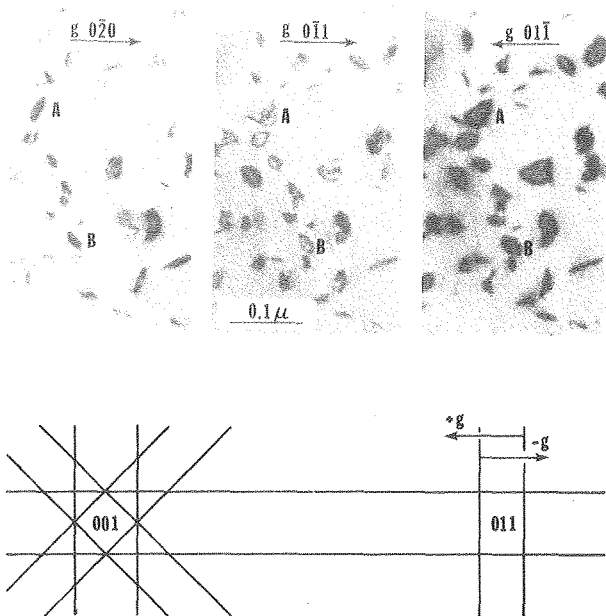


Fig. 11

XBB 790-14882

This report was done with support from the United States Energy Research and Development Administration. Any conclusions or opinions expressed in this report represent solely those of the author(s) and not necessarily those of The Regents of the University of California, the Lawrence Berkeley Laboratory or the United States Energy Research and Development Administration.